Energy Conversion and Management: X 23 (2024) 100642

Contents lists available at ScienceDirect

Energy Conversion and Management: X

journal homepage: www.sciencedirect.com/journal/energy-conversion-and-management-x

Modelling guided energy management system for a hydrogen–fuelled harbour tug

Nirmal Vineeth Menon [a,b,d], Van Bo Nguyen [e], Raymond Quek [e], Chang Wei Kang [e], Baili Zhang [e], Siew Hwa Chan [a,b,c,*]

[a] School of Mechanical and Aerospace Engineering, Nanyang Technological University, 50 Nanyang Avenue, 639798, Singapore
[b] Maritime Energy and Sustainable Development (MESD) Centre of Excellence, Nanyang Technological University, 50 Nanyang Avenue, 639798, Singapore
[c] Energy Research Institute at NTU (ERI@N), Nanyang Technological University, 1 CleanTech Loop #06-04, 637141, Singapore
[d] Seatrium (SG) Pte Ltd, 80 Tuas South Boulevard, 637051, Singapore
[e] Fluid Dynamics Department, Institute of High Performance Computing (IHPC), Agency for Science Technology and Research (A*STAR), 1 Fusionopolis Way, #16-16 Connexis, 138632, Singapore

ARTICLE INFO

Keywords:
Hydrogen tug
Hydrogen fuel cell
Hydrogen propulsion
Vessel powertrain modelling
Vessel resistance
Operational planning

ABSTRACT

The use of hydrogen as a source of fuel for marine applications is relatively nascent. As the maritime industry pivots to the use of alternate low and zero-emission fuels to adapt to a changing regulatory landscape, hydrogen energy needs to present and substantiate a technical and commercially viable use case to secure its value proposition in the future fuel mix. This paper leverages the technoeconomic and environmental assessment previously performed on HyForce, a hydrogen-fuelled harbour tug which has shown encouraging results for both technical and commercial aspects. This study aims to create a digital twin of HyForce to accurately predict her operability in real-world scenarios. The results from this study identify the strengths and drawbacks of the proposed use case. This is achieved by embedding the detailed design of HyForce in a virtual environment to further evaluate its operational performance through Computational Fluid Dynamics (CFD) simulations of realistic environmental conditions such as wind, wave, sea currents, and friction attributed to the properties of seawater. The results from this study indicate a base case power requirement of 93 kW to 1892 kW to achieve speeds of 5 to 12 knots in the absence of external environmental influences. Consequently, the speed of HyForce has a profound impact on total resistance peaking at 97.3 kN at 12 knots. Seawater properties such as low seawater temperature of 0 °C, and a high salinity of 50 g/kg increased friction. Additionally, wind speeds of 10 m/s acting on HyForce, delivered a resistance of 3 kN. However, these will be well mitigated through the design of the propulsion system which will be able to deliver a thrust power of 1892 kW and with assistance from the energy storage systems produce 2 MW of power to overcome the resistance experienced. The findings presented in this paper can serve as a foundation for constructing a robust model for the development of a predictive controller for future work. This controller has the potential to optimize the configuration of hydrogen and battery energy storage, aligning with desired cost functions.

1. Introduction

The maritime industry has historically been and still is a key enabler to support trade and commerce between countries. Shipping has been able to maintain its position of having a strong foothold in this segment despite technological advancements as it provides the best economies of scale. Sophisticated tools and algorithms have been developed in recent times to optimise the movement of freight to ensure that the maximum efficiency is extracted from each voyage. These digital tools are predominantly tailored to facilitate last-mile deliveries as they involve processing a large amount of data in a Business-to-Consumer operating model [1]. With the shift in consumer preference to purchase goods using e-commerce platforms, these tools now ensure that purchase orders are fulfilled efficiently and reliably. The important 'handshake' between last-mile deliveries and upstream production facilities places the burden on the shipping industry to meet the high expectations expected by both, the companies that produce these products and their intended customers. These expectations come in the form of lead times

* Corresponding author.
E-mail address: mshchan@ntu.edu.sg (S.H. Chan).

https://doi.org/10.1016/j.ecmx.2024.100642
Received 25 February 2024; Received in revised form 17 May 2024; Accepted 30 May 2024
Available online 31 May 2024

for delivery, due care during cargo handling and, more recently, the environmental footprint from transportation. With over 90 % of the world's cargo now transported by ships, it is clear that the maritime industry is responsible for the growth of the world's economies by providing an avenue for the cost-effective transportation of goods required to sustain the upward Gross Domestic Product (GDP) trajectory of developing countries [2].

This dominance the industry has in this sector of moving cargo can be dated back several hundreds of decades ago to the creation and use of combustion engines which was a pivotal backbone to the societal economy in the 2nd industrial Revolution. Even before this, albeit on a much smaller scale, ships with sails were carrying cargo for trade between the East and the West. Goods such as silk, tea and spices travelled to the West and in exchange, precious metals, horses, and technology were sent to the East [3]. The maritime industry has not taken this dominance for granted. Continuous improvements and innovative solutions have always been explored and implemented to ensure the optimised use of resources [4,5]. Close collaborations between key stakeholders including international bodies such as the United Nations International Maritime Organisation (IMO), governments, ports, and industry players have resulted in several revolutionary measures to optimise port management and ambitious targets to combat climate change [6–9]. To achieve this target, a substantial amount of effort is now committed to exploring the use of alternative fuels in retrospect to the longstanding use of fossil-based heavy fuel oil or marine diesel. To this effect, several Life-Cycle Assessments (LCA) of potential fuels have been conducted and published [10–13]. These assessments are guided by the standardised ISO 14040:2006 metric, which encompasses raw material acquisition, production, construction, operation, demolition, and recycling. This standard streamlines the data to ensure that it is accountable and verifiable. Furthermore, these LCAs consider several unique factors such as human health, environmental impact, and social aspects from a 'cradle to grave', which provide a holistic overview of the true impact of potential candidates to replace fossil fuels.

Of the several prospective fuel choices, the use of hydrogen is considered a promising option [14–17]. This originates from the absence of carbon atoms or other molecules that have the potential to cause global warming. More advantageously, it produces zero emissions during its lifecycle 'utilisation phase' as defined earlier. Hydrogen is currently widely used in several industries including the refining of petrochemicals, the production of ammonia as a fertilizer as well as the production of iron via the direct iron reduction method [18]. Hydrogen can be produced by several traditional and increasingly novel pathways [19–21]. However, the source of hydrogen as a feedstock is overwhelmingly derived from steam methane reforming (SMR), a fossil-based production method. Increasingly, to reduce the environmental impact of SMR, which produces carbon dioxide as a product, several production facilities are beginning to incorporate carbon capture technologies as part of their process design [22–24]. Furthermore, the cost parity between the added cost of retrofitting carbon capture technologies and the traditional SMR process has significantly reduced due to its technology maturity and cost competitiveness resulting from economies of scale [25–27]. Depending on the location of these production facilities, this delta in pricing is also managed by local carbon taxes levied on the emissions of carbon dioxide [28].

Although the use of hydrogen as fuel dates to the 1960 s as rocket fuel used in the Centaur Programme by the National Aeronautics and Space Administration (NASA), there are different challenges to the use of hydrogen in land-based scenarios such as automotive or locomotive as well as in the marine environment. Regardless of the end application, the eventual solution needs to be fit for purpose and tailor-made to address the unique attributes surrounding its use. One such use case example is the use of hydrogen for harbour tugs. In a published study in the International Journal of Hydrogen Energy, HyForce, a hydrogen-fuelled harbour tug was conceived as an alternative to traditional diesel tugs which currently dominate as the preferred choice of fuel [10]. The previous study investigated several important permutations regarding the choice of powertrains which included fuel cells and internal combustion engines (ICE), the environmental impact of the hydrogen from different sources as well as the break-even point of hydrogen (USD/kgH_2) needed to achieve cost competitiveness and commercial viability against their diesel-driven counterparts.

This paper seeks to advance the current investigation by introducing new digital elements and Computational Fluid Dynamics (CFD) modelling to further quantify and validate the viability of utilizing hydrogen as a fuel source for this specific application. A model of HyForce will be developed, transforming the harbour tug into a virtual environment conducive to a range of simulations. These simulations encompass various environmental conditions anticipated for HyForce's operation, such as wind speed, wave height, currents, seawater temperature, and salinity. There are current gaps in the literature surrounding the use of CFD tools for this intended application [29–33]. In [29], the authors have described in great detail the numerical analysis surrounding the manoeuvrability of a similar tugboat application albeit with an emphasis on the skeg of the vessel. This feature is not present in HyForce as it operates with twin azimuth thrusters. [30–32], are high-level conceptual studies on using hydrogen fuel cells with batteries for marine vessels. Collectively, these studies address different considerations surrounding the multi-faceted issue of the use of hydrogen in marine applications. This includes hydrogen availability, fuel consumption, bunkering requirements, safety and hazardous zones, electrical load analysis, and greenhouse gas emissions quantification. However, they exclude any investigation to rationalise or substantiate the required power to be delivered by the fuel cells. The current study's outcomes, which include the methodology and the framework, will address this gap to complement future studies. In [33], the CFD study performed was constrained to propellors and did not investigate their interactions with the hull of the vessel. Essentially, the power delivered by the propellor will need to compensate for the additional loads experienced on the vessel during operations. The absence of this integration will make it challenging to holistically evaluate the performance of the vessel. The modelling simulations conducted on HyForce, coupled with the theoretical model of the power trains, will yield essential inputs for power requirements under different operating conditions. These inputs are instrumental in managing operational power variations, facilitating outcomes such as (i) reduced fuel consumption, (ii) optimized battery charge cycles, (iii) improved battery charging scenarios, and (iv) setting a lower hard limit for the reserve 'take-me home' power.

2. Overview of the HyForce and designed operational missions

The HyForce used in this study is a liquid hydrogen (LH_2) fed fuel cell-powered harbour craft with batteries designed to operate within coastal waters. Of the several tasks the vessel is capable of, its main mission is to ensure safe passage, berthing and unberthing of larger vessels on tow. To fulfil this task, HyForce is equipped with a 45-ton bollard pull winch to perform the necessary pull and/or push towing scenarios. The towing winch is strategically placed at the forward section of the vessel to accede to the placement of a 50 m^3 LH_2 containment system, containing approximately 3.6 tonnes of hydrogen at the stern as seen in Fig. 1. Overall technical geometry configurations of the HyForce vessel are shown in Table 1.

The vessel has a designed combined total power of 2 MW delivered by two azimuth thrusters to deliver a total bollard pull capacity of 45 tons [10]. The thrusters are driven by electrical motors energised by fuel cells on independent powertrains. This negates any power failures on one of the powertrains and ensures that the vessel remains operable to safely transit back to shore for troubleshooting and rectification. This can be achieved by ensuring the power management system encompasses isolated breakers on the main switchboard.

Harbour crafts, unlike seagoing vessels, have a relatively unpredictable and erratic operational demand. This is ever so apparent for

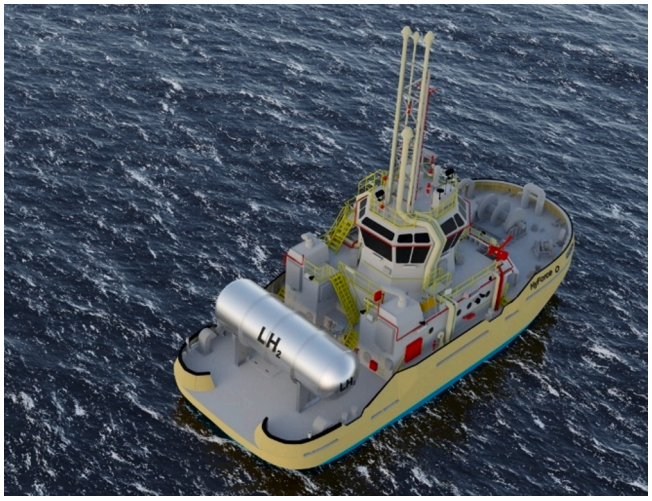

Fig. 1. Bird's-eye view of HyForce with liquid hydrogen storage tank.

Table 1
HyForce vessel parameters.

Parameter	Symbol	Value	Unit
Overall length of the tugboat	L	30	m
Width	W	12	m
Wetted surface of bare hull	S_{BH}	401	m^2
Length of water line	L_W	28.22	m
Breadth of water line	B	12	m
Draft	T	3.30	m
Displacement	∇	661	m^3
Wetted surface area of appendages	S_{APP}	5	m^2
Waterplane coefficient	C_{wp}	0.851	–
Midship section coefficient	C_m	0.854	–
Block coefficient	C_b	0.576	–
Form factor	$(1+k_1)$	0.57	–

tugboats, which provide on-demand service as required. When deployed, tugboats can perform a myriad of different operational scenarios to ensure mission success. As the tugboat transitions through the different operational scenarios, the corresponding power demand from the propulsion system changes. As no two missions are alike, the inherently dynamic nature of tugboat operations makes it challenging to accurately estimate the combined power output the propulsion systems are required to produce. In the unlikely scenario that the tugboat performs identical missions (i.e., same load demand), environmental conditions differ resulting in variations in the power required to sustain vessel speed, heading or towing force. Nonetheless, a basis of design needs to be established to right-size the propulsion system capable of fulfilling the operational demand rigour. For HyForce, the operational profile was curated through close collaboration with an existing tugboat operator in Singapore to best harmonise the different potential mission scenarios that can be anticipated. The operational profile can be seen in Table 2.

Table 2
Operating scenarios for HyForce.

Operating Scenarios	
In port – Mainly hotel loads (e.g., HVAC, lighting, pantry, etc.)	7.2 hrs (60 %)
Movement to mission location	1.8 hrs (15 %)
Awaiting mission start (i.e., hooking up of tow line etc)	1.2 hrs (10 %)
Mission execution	1.8 hrs (15 %)
Auxiliary loads	400.0 (kW)
Transit 6 knots	103.25 (kW)
Transit 10 knots	770.01 (kW)
Transit 12 knots	1601.90 (kW)
Towing 50 % (b.p)	765.5 (kW)
Towing 100 % (b.p)	2082.5 (kW)
Maximum speed	12.0 (knots)
Maximum pulling load	45.0 (ton)

3. Methodology for power evaluation

For optimal operation of the designed operating scenarios, an accurate power evaluation tool is developed. This section describes the methodology for the optimal power evaluation to achieve operational profile setting with the effects of the environment. Particularly, the effects of current and water depth directly affect the speed of the HyForce, while the surface roughness, water temperature, water properties, wind, wave, displacement, and trim directly contribute to the total resistance of the tug. The required total power is needed to overcome the total resistance and maintain the HyForce performance. Fig. 2 shows the evaluation workflow for power and tugboat performance considering the environmental effects. Details of each component are analysed in the subsequence subsections.

3.1. Speed correction

Both current speed and the depth of seawater directly influence the HyForce speed. To obtain the actual speed of the tug, the correction speed must be accurately evaluated. The effect of the water depth can be evaluated via empirical formulation [34], while the effect of the sea current can be evaluated through vector summation theory and the relative direction of the current and the tugboat. Thus, the actual speed of the tug can be expressed as

$$V_{actual} = V_{set}\left(1 - \Delta V_{depth}\right) + \Delta V_{current} \tag{1}$$

In this expression, V_{set} is the setting speed that engine(s) can deliver in calm and depth (>20 m) water. ΔV_{depth} is speed reduction caused by the depth of the seawater. $\Delta V_{current}$ is the change in tugboat speed caused by the current of the sea. V_{actual} is the corrected speed of the tugboat. This actual speed of the tug will be implemented and integrated into the programme for the toral resistance and power evaluation.

3.1.1. Effect of the water depth

HyForce, a harbour craft operates in coastal water with varying depths. The depth of water has an impact on the actual speed of the water and this speed reduction is calculated using the formulation proposed by Lackenby [35]:

$$\frac{\Delta V}{V} = 0.1242\left(\frac{C_m}{H^2} - 0.05\right) + 1 - \sqrt{\left(tanh\frac{gH}{V^{\frac{2}{3}}}\right)} \text{ for } \frac{C_m}{H^2} \geq 0.05 \tag{2}$$

where (C_m) is the midship section coefficient underwater, (g) is the gravity acceleration, (H) is water depth, (V) is the tugboat speed, and (ΔV) is the decrease of the tugboat speed due to the shallow water. From the above, water depths exceeding 20 m do not have any considerable effect on the speed reduction of the vessel.

3.1.2. Effect of the sea current

The corrected speed of the HyForce is evaluated based on the relative angle of the current direction and the tug direction (θ_c), the current velocity (V_c), and the relative velocity (V_s) of the tug and the seawater. Which, the corrected angle and corrected speed are calculated using the following formulations.

If $(90^o < \theta_c < 270^o)$:

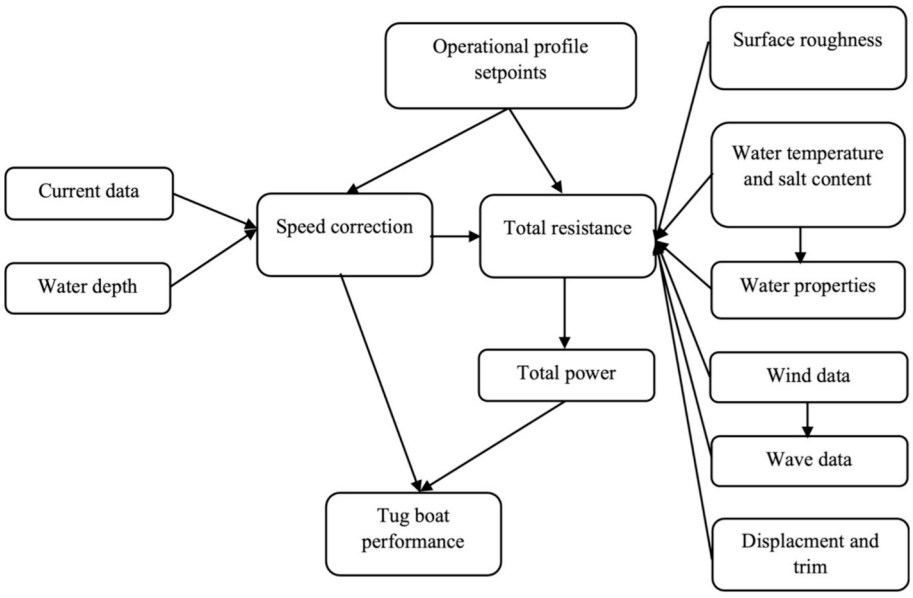

Fig. 2. Power evaluation workflow for the operational profile of HyForce with environmental effects.

$$\theta_{corrected} = 180 - tan^{-1}\left(\frac{V_c \times sin\left(\frac{\pi}{180} \times \theta_c\right)}{V_s + V_c \times cos\left(\frac{\pi}{180} \times \theta_c\right)}\right) \times \frac{180}{\pi} \tag{3.1}$$

$$\theta_{cal} = tan^{-1}\left(\frac{V_c \times sin\left(\frac{\pi}{180} \times \theta_c\right)}{V_s + V_c \times cos\left(\frac{\pi}{180} \times \theta_c\right)}\right) \tag{3.2}$$

$$V_{corrected} = V_s - \frac{V_c \times cos\left(\frac{\pi}{180} \times \theta_c\right)}{cos(abs(\theta_{cal}))} \tag{3.3}$$

else :

$$\theta_{corrected} = 180 - tan^{-1}\left(\frac{V_c \times sin\left(\frac{\pi}{180} \times \theta_c\right)}{V_s - V_c \times cos\left(\frac{\pi}{180} \times \theta_c\right)}\right) \times \frac{180}{\pi} \tag{3.4}$$

$$\theta_{cal} = tan^{-1}\left(\frac{V_c \times sin\left(\frac{\pi}{180} \times \theta_c\right)}{V_s - V_c \times cos\left(\frac{\pi}{180} \times \theta_c\right)}\right) \tag{3.5}$$

$$V_{corrected} = V_s - \frac{V_c \times cos\left(\frac{\pi}{180} \times \theta_c\right)}{cos(abs(\theta_{cal}))} \tag{3.6}$$

3.2. Effect of the temperature and salt content on seawater properties

Seawater temperature varies according to geographical location and the spectrum is sufficiently wide to affect its viscosity and density. Together with temperature, salinity is also an important parameter which contributes to the change in the physical properties of seawater. These physical properties can be calculated based on the correlation of freshwater and salinity (S_A) and temperature (T) given by Sharqawy et al. [36]. The dynamic viscosity of seawater (μ_{sw}) can be evaluated using the following equations referencing freshwater (μ_{fw}) as below.

$$\mu_{sw} = \mu_{fw}(1.0 + A^*S_A + B^*S_A) \tag{4}$$

Where A and B are functions of temperature, T in (°C) is given below:

$$A = 1.541 + 0.01998T - 9.52 \times 10^{-5}T^2 \tag{4.1}$$

$$B = 7.974 - 0.07561T + 4.724 \times 10^{-5}T^2 \tag{4.2}$$

In which, the viscosity of the freshwater is the function of the temperature and be expressed as

$$\mu_{fw} = 0.0018 - 6.0 \times 10^{-5}T + 1.0 \times 10^{-6}T^2 - 8.0 \times 10^{-9}T^3 \tag{4.3}$$

The density of the seawater is expressed using the following correlation

$$\rho_{sw} = \rho_{ref} + B1^*S_A + 1.5^*C1^*S_A + d_0^*S_A^2 \tag{5}$$

where

$$\rho_{ref} = a_0 + a_1T + a_2T^2 + a_3T^3 + a_4T^4 + a_5T^5 \tag{5.1}$$

$$B1 = b_0 + b_1T + b_2T^2 + b_3T^3 + b_4T^4 \tag{5.2}$$

$$C1 = c_0 + c_1T + c_2T^2 \tag{5.3}$$

In these expressions, the coefficients a_i, b_i, and c_i are given as

$a_0 = 999.842594$, $a_1 = 6.793953E-2$; $a_2 = -9.095290E-3$, $a_3 = 1.001685\ E-4$, $a_4 = -1.120083E-6$, $a_5 = 6.536332E-9$, $b_0 = 8.2449\ E-1$, $b_1 = -04.0899E-3$, $b_2 = 7.6438E-5$, $b_3 = -8.2467E-7$, $b_4 = 5.3875\ E-9$, $c_0 = -5.7246E-3$, $c_1 = 1.0227E-4$, $c_2 = -1.6546E-6$, $d_0 = 4.8314E-4$.

The calculated seawater properties as a function of temperature and salinity show that the seawater density is highest when the temperature is at 0 °C with a corresponding salt concentration of 50 g/kg seawater.

3.3. Total resistance

This section studies all the key parameters contributing to the total resistance of HyForce. The implications of (i) wind, (ii) water, (iii) wave data, and (iv) friction on the total resistance acting on HyForce were investigated. The methodology is to isolate and quantify the impact of each parameter on the total resistance applied to HyForce. The effects of wind and water are evaluated through computational fluid dynamics, while the effects of the wave and friction are computed using empirical methods. These environmental effects are anticipated to be observed on

HyForce during operations and inevitably have an impact on the total power required. It is hence prudent to design any power management optimisation strategies against a realistic real-world scenario.

3.3.1. Wind resistance

An environmental attribute that can contribute significantly to ship motions during operations is the presence of wind. This is more pronounced for smaller vessels and HyForce falls under this category. To this effect, CFD can play an important role in evaluating the impact of wind load on the vessel. The results generated from the CFD are useful to understand the complex airflow behaviour around the vessel. Through modelling and simulation, the wind resistance acting on HyForce can be quantified and analysed. A fit-for-purpose approach was taken to simplify the complex superstructure which otherwise require a detailed and locally very fine grid which might not necessarily add significant improvement to the accuracy of the results. A modified geometry of the model was used to identify any blockage effects. The physical dimensions of HyForce were the length (L_W) of 28.22 m, breadth (B) of 12.0 m, the frontal projected area (A_F) of 130.2 m^2, lateral projected area (A_L) of 253.5 m^2. Also, the reference wind velocity (U_{ref}) of 10.0 m/s was used with a Reynolds number of $7.76x10^6$. The computational domain and direction of wind experienced on the vessel are given in Fig. 3.

The CFD calculations were based on a geometry model that represented HyForce on a 1:1 scale where the wind loading coefficients, $C_{FX} = \frac{F_x}{\frac{1}{2}\rho V^2 A_F}$, $C_{FY} = \frac{F_y}{\frac{1}{2}\rho V^2 A_F}$ and $C_M = \frac{M_x}{\frac{1}{2}\rho V^2 A_F L_{OA}}$ are defined through the forces (F_x and F_y) in the x and y direction with the moment (M_x) on the tugboat in the z direction around the centre of the vessel. The top surface of the computational domain is 40 m from the water surface which is sufficiently high enough to capture the full effect of wind flow over HyForce as illustrated in Fig. 3.

The computational grids are constructed using Ansys Fluent and the higher-order unconstructed Quadratic Upstream Interpolation for Convective Kinematics (QUICK) numerical scheme is employed for the space discretization of the Reynolds-averaged Navier-Stokes (RANS) governing equations. The shear stress transport (SST) k-ω turbulence model [37] is used together with an automatic wall function approach for a full boundary layer resolution [38]. The velocity profile, $U(z)$, is specifically chosen to resemble best an atmospheric boundary layer profile observed in open seas [39]. The moment coefficients are calculated at different inflow angles from 0.0 degrees to 360.0 degrees with a step increase of 10.0 degrees. The wind speed is set at 10.0 m/s at the inflow boundary with constant pressure specified downstream of the computational domain. 36 simulations were performed to evaluate the moment coefficients with a total mesh count of about 3.5 million obtained from the mesh convergence study. The results from the CFD calculations for both the longitudinal and lateral wind load coefficients are shown in Fig. 4.

Fig. 5 shows the velocity contours at the cross-section of HyForce at 0.0 deg heading (wind blowing from the back) and 180.0 deg heading (wind blowing from the front). The obtained results show that the wind speed slows down as it approaches the tugboat and a wake is created as it leaves. This creates a high pressure in the frontal direction and a low pressure in the wake region which is illustrated in Fig. 6.

3.3.2. Water resistance – Currents

Similarly, water resistance is an important factor contributing to the total resistance, which is also evaluated through the modelling simulation of the incompressible flow using computational fluid dynamics. The QUICK numerical scheme is employed for spatial discretization of the incompressible water flow, which is governed by RANS equations. The SST k-ω model is used for the turbulence model and details of the numerical method are extracted from Yuck et al [40]. A total of 36 CFD simulations were performed with varying seawater current headings from 0.0 degrees to 360.0 degrees in increments of 10.0 degrees using the finite volume method within Ansys Fluent. The computational domain is determined to ensure that the far-field boundary conditions do not affect the accuracy of the results. A mesh grid with a total of about 4.0 million cells obtained from mesh grid convergence studies was used in the simulation. The seawater properties that best represent Singapore's coastal waters were chosen, which set the temperature at 25℃ and salt concentration at 35 g/kg seawater, respectively. This simulation is performed at a speed of 1.0 knot, equivalent to 0.513 m/s at a Reynolds value of 6.92x106. The water load coefficients of the longitudinal and lateral forces are calculated similarly to wind resistance and their results are shown in Fig. 7.

The simulations performed provided the velocity and pressure contours across HyForce and the results are shown in Fig. 8 and Fig. 9 respectively. Fig. 8 shows the velocity contour at the middle cross-section of the tugboat for the different current heading directions. Fig. 8 (a) shows the velocity contour of the 0.0 degrees, and Fig. 8 (b) shows the velocity contour for the case of 180.0 deg. Fig. 9 shows the pressure contour of the seawater on the surface of the tugboat for different current heading directions. Fig. 9 (a) is the case when the current heading direction is at 0.0 degrees, and Fig. 9 (b) is the case of 180.0 degrees.

3.3.3. Wave resistance – Heave & pitch

To determine the added resistance that will be experienced by HyForce due to waves can be determined by model testing in a tank basin. This controlled environment is capable of artificially replicating waves accurately to capture and record the observations and results on the test model. Alternatively, an approximation formula which is limited to ± 45.0 degrees off the bow can be used given in the equation below [41]:

$$R_{AWL} = \frac{1}{16}\rho g H_w^2 B\sqrt{\frac{B}{L_{BWL}}} \tag{6}$$

The resistance attributed to waves (R_{AWL}) is a function of the significant wave height (H_w), the breadth (B), and the length of the bow on the water line (L_{BWL}) of 7.4 m. The range of the wave height is selected through the actual condition of the wind and history measurement data for the Singapore Strait. Compared to the water resistance, waves contribute significantly less to the overall total resistance experienced by HyForce during operations.

3.3.4. Friction resistance

The friction resistance is a function of seawater properties (density and viscosity) and the surface roughness of the hull. The estimated formulation of the friction resistance is given in ref [8] as

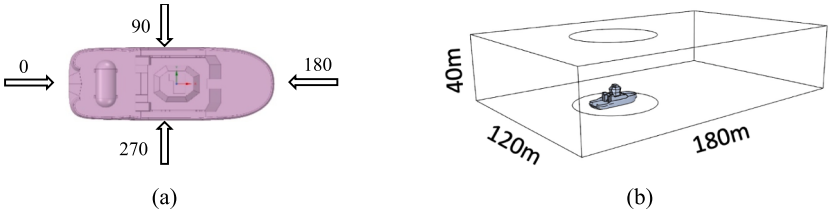

(a) (b)

Fig. 3. Numerical setup and direction definition of the force: (a) Direction of wind acting on the vessel, (b) designed computational domain for CFD calculations.

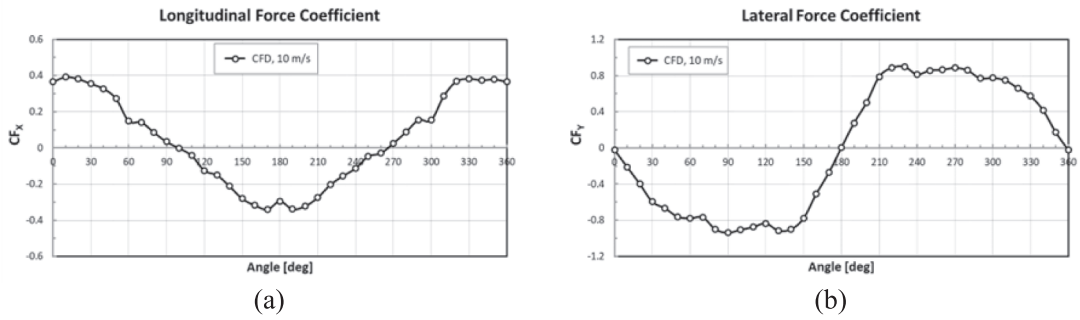

Fig. 4. Wind load coefficients at different wind heading directions (a) Longitudinal (b) Lateral.

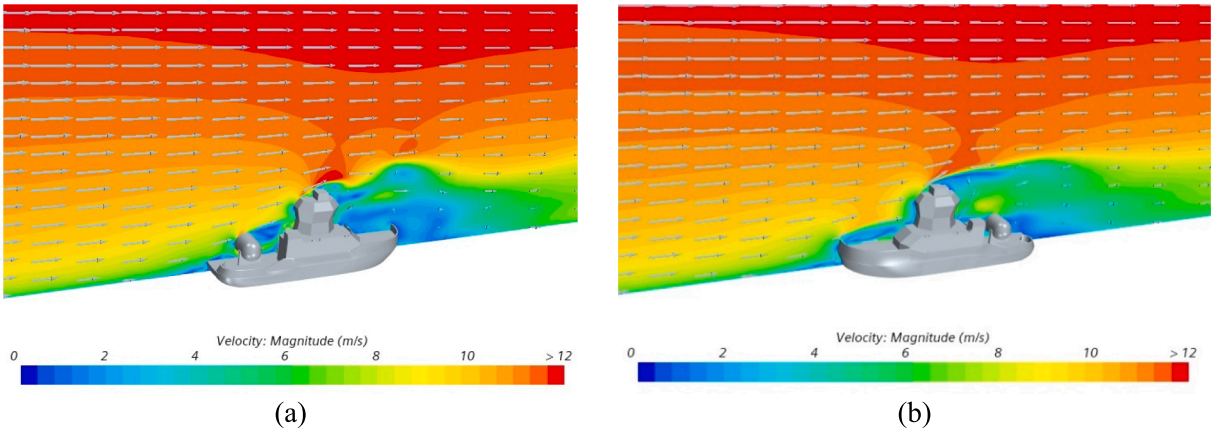

Fig. 5. Wind velocity contour including the wake for different wind heading directions (a) 0.0 degrees (b) 180.0 degrees.

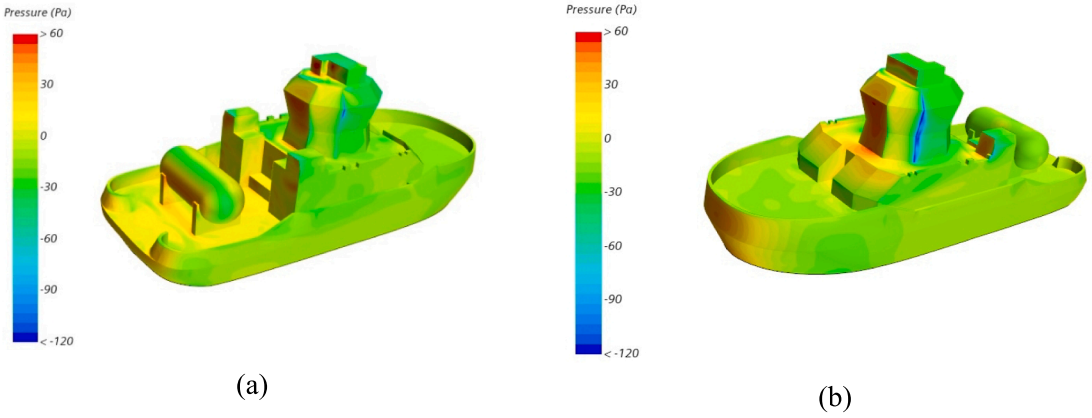

Fig. 6. Pressure contour acting on HyForce's walls for different wind heading directions (a) 0.0 degrees (b) 180.0 degrees.

$$R_F = \frac{1}{2}\rho(S + S_{APP})V_S^2 C_F \tag{7}$$

In this expression, C_F is the friction coefficient, ρ is the density of the seawater, S is the wetted area of the tugboat's hull, S_{APP} is the wetted surface area of the appendages, V_s is the velocity of the HyForce. The friction coefficient is calculated as

$$C_F = C_{F0}*(1.0 + k) + C_{SR} \tag{7.1}$$

The reference frictional resistance coefficient is calculated as

$$C_{F0} = \frac{0.075}{(log(Re) - 2.0)^2} \text{ with } Re = \frac{V*L_{WL}}{\mu} \tag{7.2}$$

The coefficient of the surface roughness is calculated as

$$C_{SR} = 0.001\left(105\left(\frac{ks}{L_{WL}}\right)^{1/3} - 0.64\right) \tag{7.3}$$

In this study, $k = 0.57$, $ks = 120 \times 10^{-6}$, and $\rho = 1025.9$ kg/m^3, $S = 408$ m^2, $L_{WL} = 28.2$ m, and $\mu = 1.831 \times 10^{-5} Pa.s$ (corresponding with the Singapore Strait seawater properties). The appendage resistance is largely contributed by the twin azimuth thrusters which provide both the power for propulsion and manoeuvrability. This results in higher friction as the vessel speed increases. The roughness is contributed by rust, buckling, welding beads, paint roughness, and marine growth. The assumptions to calculate the frictional resistance include a clean hull with no marine growth present. Also, the model excludes any silicon-

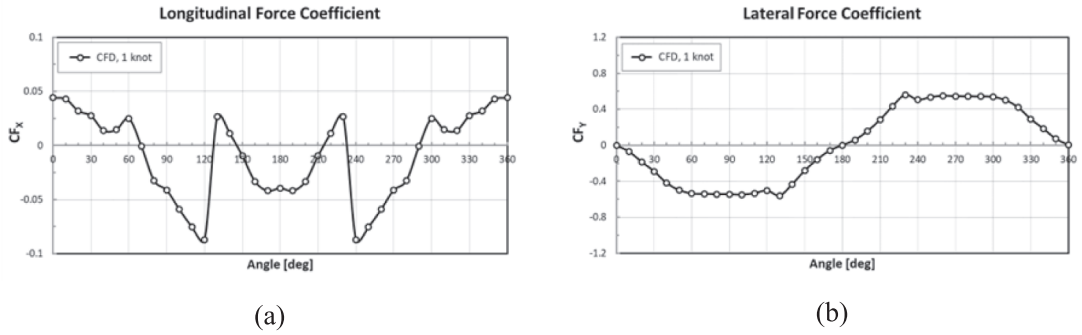

Fig. 7. Current load coefficients at different current heading directions; (a) Longitudinal coefficient and (b) Lateral coefficient.

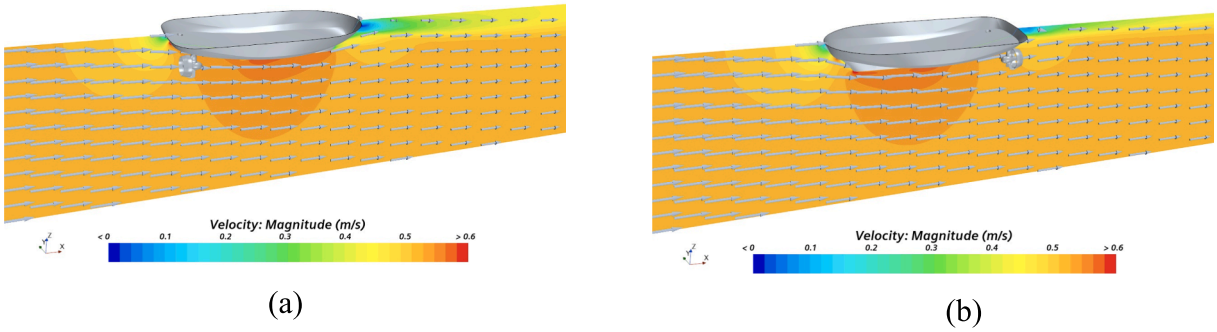

Fig. 8. Velocity contour at the cross-section along the centreline of HyForce at different current headings with a speed of 1 knot (a) 0.0 degrees (b) 180.0 degrees.

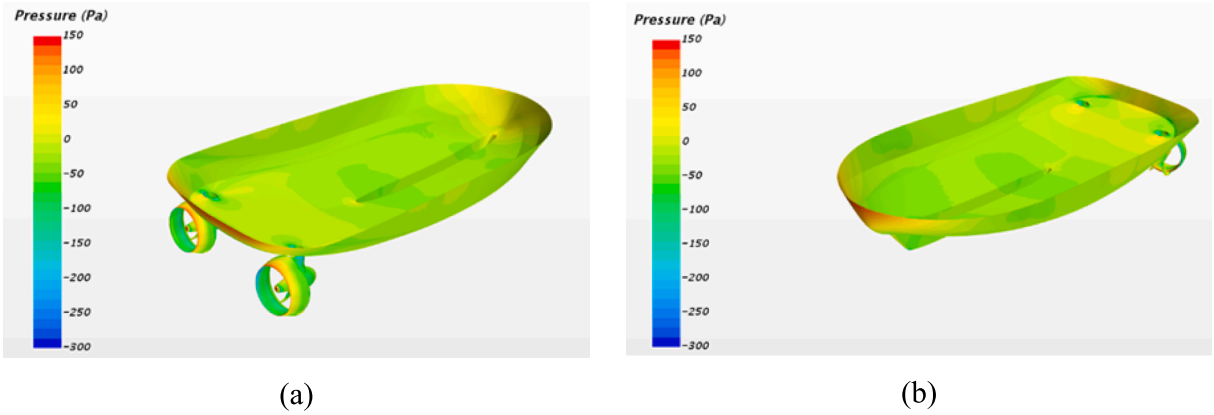

Fig. 9. Pressure contour at the cross-section along the centreline of HyForce at different current headings with a speed of 1 knot (a) 0.0 degrees (b) 180.0 degrees.

based paint coating system on the hull, which is designed to reduce friction. The above assumptions are valid as marine growth is managed and mitigated through the application of antifouling paint, which is typical for most if not all marine vessels as well as drydocking of HyForce at regular intervals as prescribed by classification society requirements. It should be noted that the surface roughness of the hull will be changed during the operation time of the tug. The new hull often has roughness around 120–160 mm, while it will be up to 300–400 mm before maintenance is needed.

3.3.5. *Total resistance and validation*

The total resistance (R_{Total}) acting on HyForce is a summation of several mentioned contributing factors. As a vessel moves through the water, two evident characteristics are apparent from observation. The wave pattern that moves with the hull and the turbulent flow along the length of the ship becomes a wake at the stern. These water flow traits, therefore, contribute resistance to the moving vessel. Predominantly, the total energy dissipated concerning losses from resistance can be classified into two main contributing factors, (i) pressure and (ii) friction. Pressure, which accounts for the normal forces acting on the hull can be attributed to hydrodynamic components and the energy in wave breaking, wave pattern, and transom drag. The latter includes the viscous hull resistance resulting from skin friction against the hull of the ship and the appendages (e.g., the rudder, and azimuth thrusters which protrude out of the hull) [42]. Particularly, the wind also greatly contributes to the total resistance acting on the top structure of the tugboat, while the water contributes to the total resistance by both pressure and friction acting on the hull of the tug. The wave resistance acts on the hull and strongly depends on the wave height. The friction resistance value is the function of the hull's surface roughness and the seawater viscosity. Adding to the resistance acting against the vessel is given in the following equation [43].

$$R_{Total} = R_{wind} + R_{water} + R_W + R_F \quad (8)$$

For the validation of the current methodology, the current calculated resistance is compared with the predicted total resistance based on the measurement data of the model for the same operational and environmental conditions with the velocity of the vessel from 7 knots to 12 knots. Particularly, a model of the vessel with the appendages is tested in the calm water tank to determine the resistance characteristics. The hull model was manufactured according to the requirement given in the ITTC recommended procedure 7.5–01–01–01 for the ship models [44]. The propeller(s) model was manufactured according to the requirements given in the ITTC recommended procedure 7.5–01-02–02 for propeller model accuracy [44]. The methods used to carry out the tank tests and to extrapolate the results for the actual vessel follow the general methodology given in the relevant ITTC recommended procedures [44]. The tests are carried out in the deep-water towing tank size of 270.0 m × 12.0 m × 6.0 m corresponding with the length, breadth, and depth, respectively. The tests are carried out in the seawater properties of 3.5 % salinity and temperature of 15 °C. The modelling and simulations are carried out for the same operational and environmental conditions. The wind and current direction are $\theta_{wind} = 0$ and $\theta_{current} = 0$. The obtained results are plotted together in Fig. 10 for the comparison. The observation indicates that our model is in good agreement with the measurement-based extrapolation result. A maximum difference between the current modelling method and measurement-based extrapolation value is about 6.5 % is observed. It implies that our model can be used to accurately predict the total resistance acting on the HyForce to estimate the optimum power required for vessel operation.

3.4. Propulsion evaluation

The propulsive forces that are required for HyForce to achieve the required operational requirement ($F_{Operational}$) are subject to several external factors that influence the overall power required to be delivered to the propeller. This interaction occurs between the hull and the propeller and includes components such as (i) wake fraction, (ii) thrust deduction fraction, and (iii) relative rotative efficiency. Through the computation of these variables, the torque and thrust of each propeller, total delivered power, and the propeller efficiency can be determined.

The wake fraction (ω) is a variable that predicts the efficiency and thrust of the propeller when operating in the ship's wake. The wake which has a complex flow form will inevitably result in a lower average speed of water flowing into the propeller compared to the speed of advance of the hull. The ratio of the advance coefficient of the propeller

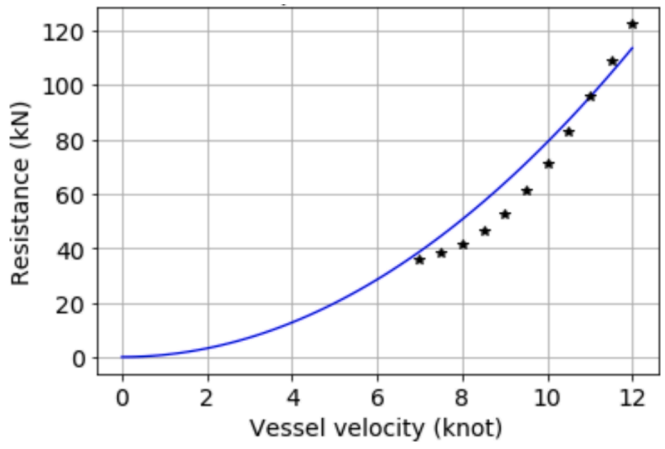

Fig. 10. Validation of the current method (solid blue line) with measurement data (black stars) under the same operating and environmental conditions for different vessel speeds. (For interpretation of the references to colour in this figure legend, the reader is referred to the web version of this article.)

(J_p) and of the hull (J_h) will give the wake fraction as shown:

$$\omega = 1 - (J_p/J_h) \quad (9)$$

During the operation, the HyForce manoeuvres using her dedicated propulsion system, the spinning of the azimuth thrusters, located at the stern of the vessel, disrupts the pressure fields at the rear of the hull as the propellers accelerate the flow of water in this region. This causes an increase in shear force (i.e., frictional resistance) because of the increased movement of water molecules in the boundary layer between the hull and seawater. Therefore, the thrust generated will minimally need to exceed the bare hull resistance. The thrust deduction fraction (t) arguably can be described as a resistance augment instead of a propulsive force but not in practice. It can be calculated using equation (10).

$$t = 1 - (R_{Total} - F_D)/(N_p \times Th) \quad (10)$$

Most vessels are propelled using a single propeller designed sufficiently large to provide the necessary thrust (Th). HyForce, limited by her size, is propelled using twin screws to deliver the required power, which inadvertently has an impact on the pressure fields at the stern of the vessel and hence necessitates the inclusion of the number of propellers (N_p) in the overall equation.

The propeller, which is connected via a shaft to the main engines or motors is supplied with the necessary torque to deliver the required thrust. To determine the intrinsic hydrodynamic performance of a propeller, model scale open water tests are performed. In these tests, the inflow of water to the model-scale propeller is uniform. The propeller efficiency (η_P) is determined by the advance coefficient of the propeller (J_p), torque coefficient (K_{Qo}), and thrust coefficient (K_T) given by:

$$\eta_P = J_p \times K_T/(2\pi \times K_{Qo}) \quad (11)$$

where the torque coefficient is:

$$K_{Qo} = \frac{Q}{\rho n^2 D^5} \quad (11.1)$$

and thrust coefficient is:

$$K_T = \frac{T}{\rho n^2 D^4} \quad (11.2)$$

However, in actual operation, the turbulent inflow of water (i.e., wake) to the propeller depends on the ship's design (i.e., hull form) to which it is fitted. Inevitably, the torque absorbed by the propeller in an open water test (K_{Qo}) differ from a similar operating condition under turbulent flow (K_{QS}), which provides the relative rotative efficiency (η_R) and it is given by:

$$\eta_R = K_{Qo}/K_{QS} \quad (11.3)$$

Having derived the (i) wake fraction, (ii) thrust deduction fraction, and (iii) relative rotative efficiency above, the torque, thrust and total delivered powered by the propellers can be determined.

The amount of thrust in kilonewtons (kN) that can be generated from HyForce as a result of the propeller's rate of revolution (RPM) (n), and diameter (D) is given by:

$$T = J_p^2 \times \rho \times D^4 \times n \quad (12)$$

The thrust produced by the propeller is accredited to the torque supplied by the shaft to which it is connected. This shaft as highlighted earlier, is driven by power-producing equipment on board and in the case of HyForce, comes from large electrical motors energized by fuel cells. The torque produced by the shaft (Q) is given by:

$$Q = (\frac{K_{QS}}{\eta_R}) \times \rho \times D^5 \times n^2 \quad (13)$$

Finally, the total delivered power by the propellers (P_D) in kilowatts (kW) can be determined by:

$$P_D = N_p \times 2\pi \times n \times Q \quad (14)$$

4. Results and discussion

4.1. Total resistance evaluation

For the total resistance, the approach to determining the various forces acting on HyForce is to first define the material parameters given in the above section. These input parameters provide the necessary estimation to investigate the total resistance acting on HyForce, which was validated in the previous section. It provides insightful information on the change in resistance and the various parameters contributing to it. This association allows for deeper analysis to inquire into the fundamentals governing the total resistance acting on a vessel. The calculated results show an increasing trend of resistance as the vessel increases in speed. Furthermore, the increment in resistance becomes more apparent as the vessel increases speed from 8 knots. This coincides with an increase in the Froude number which is a function of wave resistance. Wave resistance has a profound impact on the total resistance, and this can be attributed to the absence of a bulbous bow commonly present in larger marine vessels. The purpose of the bulbous bow, when designed optimally, reduces the total resistance and power requirement allowing for improved operational efficiency, reduced fuel consumption and better stability [45–47]. The frictional coefficient, which is a function of the Reynolds number decreases as the flow through the hull becomes more turbulent (i.e., higher Reynolds number and surface roughness of the hull). Within the turbulent region, the viscous hull resistance attributed to the boundary layer between the hull surface and moving water decreases, which results in a smaller frictional coefficient [48–50]. HyForce is a partially submerged vessel with a draft of 3.3 m. At 5 knots, the Froude number exceeds the benchmark threshold of 0.25, which indicates a significant influence of wake-making and inertia of the fluid (i.e., seawater) on the total resistance [29,51].

4.2. Propulsion and power evaluation

Similarly, the propulsion and power calculations require intrinsic properties of HyForce, which include the characteristics and performance of the propeller as well as the total resistance acting on the vessel. The characteristics of the propeller include the number of blades, diameter, and pitch ratio, while the performance of the propeller is given by its wake fraction, advance coefficient, and propeller efficiency respectively. This information is given in Table 3 and Table 4 respectively. The information is provided by the propeller's vendor, which is measured in the calm water tank tests for different vessel speeds (5.0–12.0 knots) and water properties ($\rho_{sw} = 1.025$ kg/m^3 and $\mu_{sw} = 1.0 \times 10^{-6}$ m^2/s).

The dimensionless propeller's advance ratio is the distance moved by the vessel normalised by the propeller's diameter in one revolution. From Table 4, it is observed that the propeller's advance ratio decreases as the vessel's speed increases. This reduction can be rationalised by external factors restricting the forward movement of the vessel and it is corroborated by an increase in the vessel's total resistance with increasing speed.

The wake fraction remains relatively constant throughout the different speeds which indicates that the delta between the water velocity seen by the propeller, and the hull speed does not change significantly. The low wake fraction of 0.02 highlights the uniformity of water velocity across the vessel and this can be attributed to the low block coefficient of 0.576. The ample space within the rectangular block allows for the displaced volume of water to regain an even distribution eliminating any cross flows.

The propeller's efficiency is influenced by the thrust and torque coefficients and the propeller's advance ratio. It can be misconstrued that an overwhelmingly large contributor affecting the efficiency of the propeller will be the advance ratio (i.e., distance moved by the vessel per RPM). From Table 4, it is shown that there is an opposite trend between the propeller's advance ratio and efficiency as the vessel's speed increases. The improvement of the propeller's efficiency as the vessel increases its speed is a result of bigger thrust and torque coefficients and this is validated in Table 5. The change in the thrust and torque coefficients indicates a large change in delivered thrust and torque, respectively, with a relatively smaller change in the propeller's RPM as observed from equations (13) and (14).

The total power delivered at various speeds, as detailed in Table 5 and visually depicted in Fig. 11, reveals a noteworthy trend. The curve's gradient experiences a pronounced increase at speeds surpassing 10.0 knots, primarily attributable to the heightened power delivery by the propeller. This observation finds reinforcement in the concurrent rise of the thrust coefficient within a similar operational range. The evaluated results of power, thrust, and torque are suitable and fit well with the design purpose of the current propulsion system. Especially, the calculated 1892.0 kW delivered power robustly indicates HyForce's capability to meet the designated power requirement of 2.0 MW. To ensure the attainment of the desired propeller RPM across different speeds, a detailed analysis of a suitable gear reduction ratio becomes imperative. Typically, motor generators operate at RPMs exceeding 1000, and based on the insights gleaned from Table 5, a recommended gear reduction ratio of 6.3 emerges. This strategic choice ensures a motor generator rating that sufficiently delivers the required power even under the most demanding load conditions.

Table 3
The design information of the propeller(s) used for HyForce.

Parameter	Symbol	Value	Unit
Number of propellers	N_p	2	–
Number of blades	N_b	4	–
Propeller diameter	D	2.5	m
Propeller pitch ratio	R_{p_p}	0.95	–

Table 4
HyForce's propeller design performance.

V[knots]	Wake fraction [ω]	Propeller Adv ratio [J_p]	Propeller Efficiency [η_p]
5.0	0.021	0.703	0.262
6.0	0.020	0.701	0.266
7.0	0.022	0.7	0.269
8.0	0.021	0.697	0.281
9.0	0.022	0.686	0.310
10.0	0.024	0.671	0.348
11.0	0.026	0.652	0.384
12.0	0.025	0.641	0.402

Table 5
Prediction of the total required power, thrust, and torque for the vessel operating at different speeds.

V[knots]	P_D[kW]	n[rpm]	T[kN]	Q[kNm]
5.0	93	86.1	4.8	5.2
6.0	163	103.5	7.0	7.5
7.0	259	120.7	9.7	10.3
8.0	399	138.8	13.7	13.7
9.0	605	158.4	20.5	18.2
10.0	914	179.8	31.5	24.3
11.0	1353	202.9	47.5	31.9
12.0	1892	225.3	63.7	40.1

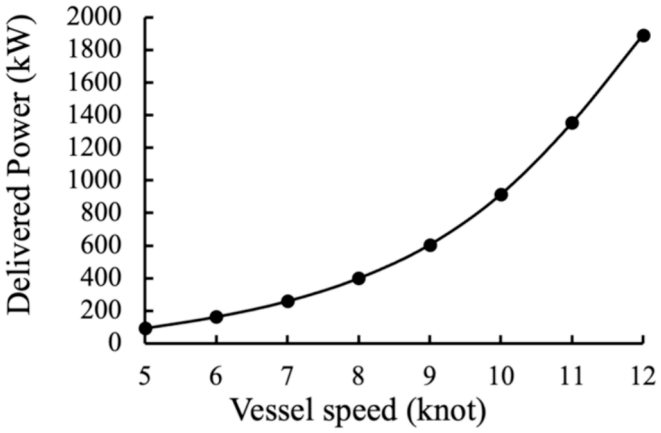

Fig. 11. HyForce power prediction for different vessel speeds within the Singapore Strait.

5. Conclusion

HyForce, a hydrogen-fuelled tugboat was designed and conceptualised to address the need for potential solutions to decarbonise the harbour craft segment of the maritime industry. The tug can be powered by fuel cells with a total delivered power of 2 MW. To further investigate the overall performance characteristics of HyForce, this study quantified the propulsion and power prediction and total resistance acting on the vessel.

The meticulous calculations of propulsion and power consider the total resistance, incorporating insights from CFD simulation and empirical methods, with a specific focus on dynamic environmental conditions. Notably, the study identifies vessel speed as a pivotal factor influencing total resistance, exhibiting a tenfold increase from 5 knots, registering at 7.2 kN, to 11.0 knots, reaching 73.1 kN. Moreover, the examination of appendages on the hull suggests their limited contribution to overall resistance.

Further exploration encompasses the impact of seawater depth, properties, wind, and waves on HyForce's resistance during deployment. CFD simulation studies reveal that the viscosity of seawater becomes a significant contributor when temperatures drop below 15 °C. Wind resistance at a speed of 10.0 m/s, particularly from headwind (0.0 degrees or 360.0 degrees), contributes 3.0 kN, posing a potential constraint on HyForce's maximum speed of 12.0 knots. Shallow seawater depth below 10 m in coastal waters is identified as an inevitable limiting factor.

The propeller design is scrutinized to ensure it generates sufficient thrust to overcome inherent resistance, facilitating optimal performance across various operational profiles. Results indicate that two propellers with a 2.5 m diameter each are adequate, delivering 1892.0 kW, with the remaining power to meet the 2.0 MW stipulation contributed by the onboard energy storage system through peak shaving.

The digital twin and modelling and simulation framework established for HyForce in this study serves as a foundation and valuable tool for the development of a model predictive controller for onboard power management. The approach to incorporating a closed-loop controller aims to ensure that the desired power reference is dynamically and optimally tracked while executing embedded power management strategies. The development direction of this controller will be designed to track the targeted cost functions material to the end user. This includes (i) lengthening the refuelling intervals, (ii) minimising the charge cycles of batteries (iii) reducing the well-to-wake emissions or other desired parameters.

This controller, once implemented, ensures the optimization of hydrogen energy by accurately representing environmental conditions and inherent resistance forces acting on HyForce. By embedding these insights into the controller's design, the study ensures that optimized outputs align with the envisaged operating scenarios for which HyForce is purposefully designed.

CRediT authorship contribution statement

Nirmal Vineeth Menon: Writing – original draft, Methodology, Investigation, Formal analysis, Conceptualization. **Van Bo Nguyen:** Writing – original draft, Supervision, Software, Data curation. **Raymond Quek:** Data curation. **Chang Wei Kang:** Writing – review & editing, Supervision. **Baili Zhang:** Software. **Siew Hwa Chan:** Writing – review & editing, Supervision.

Declaration of competing interest

The authors declare that they have no known competing financial interests or personal relationships that could have appeared to influence the work reported in this paper.

Data availability

The authors do not have permission to share data.

Acknowledgements

This research project is funded by the Economic Development Board of Singapore under the Industrial Postgraduate Programme (EDB-IPP) and by A*STAR under its RIE2025 Industry Alignment Fund – Industry Collaboration Project (IAF-ICP) I2101E0003.

References

[1] Acciaro M, et al. Environmental sustainability in seaports: a framework for successful innovation. Marit Policy Manag 2014;41(5):480–500.
[2] Testik MC, Sarikulak O. Change points of real GDP per capita time series corresponding to the periods of industrial revolutions. Technol Forecast Soc Chang 2021;170:120911.
[3] Yang J, et al. Evolution of energy and metal demand driven by industrial revolutions and its trend analysis. Chin J Popul Resour Environ 2021;19(3):256–64.
[4] Shahbakhsh M, Emad GR, Cahoon S. Industrial revolutions and transition of the maritime industry: The case of Seafarer's role in autonomous shipping. Asian J Shipp Log 2022;38(1):10–8.
[5] Watanabe MDB, et al. Drop-in and hydrogen-based biofuels for maritime transport: Country-based assessment of climate change impacts in Europe up to 2050. Energ Conver Manage 2022;273:116403.
[6] Iris Ç, Lam JSL. A review of energy efficiency in ports: Operational strategies, technologies and energy management systems. Renew Sustain Energy Rev 2019;112:170–82.
[7] Panayides PM, Parola F, Lam JSL. The effect of institutional factors on public–private partnership success in ports. Transp Res A Policy Pract 2015;71:110–27.
[8] Bach H, Hansen T. IMO off course for decarbonisation of shipping? Three challenges for stricter policy. Mar Policy 2023;147:105379.
[9] Oberthür S. Institutional interaction to address greenhouse gas emissions from international transport: ICAO, IMO and the Kyoto Protocol. Clim Pol 2003;3(3):191–205.
[10] Menon NV, Chan SH. Technoeconomic and environmental assessment of HyForce, a hydrogen-fuelled harbour tug. Int J Hydrogen Energy 2022;47(10):6924–35.
[11] Chen Z, Lam JSL. Life cycle assessment of diesel and hydrogen power systems in tugboats. Transp Res Part D: Transp Environ 2022;103:103192.
[12] Bilgili L. Comparative assessment of alternative marine fuels in life cycle perspective. Renew Sustain Energy Rev 2021;144:110985.
[13] Tomos BAD, et al. Decarbonising international shipping – A life cycle perspective on alternative fuel options. Energ Conver Manage 2024;299:117848.
[14] Latapí M, Davíðsdóttir B, Jóhannsdóttir L. Drivers and barriers for the large-scale adoption of hydrogen fuel cells by Nordic shipping companies. Int J Hydrogen Energy 2023;48(15):6099–119.
[15] Johnston C, et al. Shipping the sunshine: An open-source model for costing renewable hydrogen transport from Australia. Int J Hydrogen Energy 2022;47(47):20362–77.
[16] Inal OB, Zincir B, Deniz C. Investigation on the decarbonization of shipping: An approach to hydrogen and ammonia. Int J Hydrogen Energy 2022;47(45):19888–900.

[17] Temiz M, Dincer I. Techno-economic analysis of green hydrogen ferries with a floating photovoltaic based marine fueling station. Energ Conver Manage 2021; 247:114760.
[18] Gusev AL, et al. Production of hydrogen and carbon in the petrochemical industry by cracking of hydrocarbons in the process of heat utilization in steel production. Int J Hydrogen Energy 2023;48(40):14954–63.
[19] Farhana K, Shadate Faisal Mahamude A, Kadirgama K. Comparing hydrogen fuel cost of production from various sources - a competitive analysis. Energ Conver Manage 2024;302:118088.
[20] Ata S, et al. Thermo-enviro-economic analysis of different power cycle configurations for green hydrogen production from waste heat. Energ Conver Manage 2024;301:118072.
[21] Ren Y, et al. Modelling and capacity allocation optimization of a combined pumped storage/wind/photovoltaic/hydrogen production system based on the consumption of surplus wind and photovoltaics and reduction of hydrogen production cost. Energ Conver Manage 2023;296:117662.
[22] Ali Khan MH, et al. A framework for assessing economics of blue hydrogen production from steam methane reforming using carbon capture storage & utilisation. Int J Hydrogen Energy 2021;46(44):22685–706.
[23] Okeke IJ, Saville BA, MacLean HL. Low carbon hydrogen production in Canada via natural gas pyrolysis. Int J Hydrogen Energy 2023;48(34):12581–99.
[24] Oni AO, et al. Comparative assessment of blue hydrogen from steam methane reforming, autothermal reforming, and natural gas decomposition technologies for natural gas-producing regions. Energ Conver Manage 2022;254:115245.
[25] Arnaiz del Pozo C, Cloete S, Jiménez Álvaro Á. Carbon-negative hydrogen: Exploring the techno-economic potential of biomass co-gasification with CO2 capture. Energ Conver Manage 2021;247:114712.
[26] Liu J, et al. Evaluation and improvements on the flexibility and economic performance of a thermal power plant while applying carbon capture, utilization & storage. Energ Conver Manage 2023;290:117219.
[27] Riley J, et al. Technoeconomic analysis for hydrogen and carbon Co-Production via catalytic pyrolysis of methane. Int J Hydrogen Energy 2021;46(39):20338–58.
[28] Perey P, Mulder M. International competitiveness of low-carbon hydrogen supply to the Northwest European market. Int J Hydrogen Energy 2023;48(4):1241–54.
[29] Piaggio B, Villa D, Viviani M. Numerical analysis of escort tug manoeuvrability characteristics. Appl Ocean Res 2020;97:102075.
[30] Klebanoff LE, et al. Comparative study of a hybrid research vessel utilizing batteries or hydrogen fuel cells. Int J Hydrogen Energy 2021;46(76):38051–72.
[31] Madsen RT, et al. Feasibility of the Zero-V: A zero-emissions hydrogen fuel-cell coastal research vessel. Int J Hydrogen Energy 2020;45(46):25328–43.
[32] Melideo D, Desideri U. The use of hydrogen as alternative fuel for ship propulsion: A case study of full and partial retrofitting of roll-on/roll-off vessels for short distance routes. Int J Hydrogen Energy 2024;50:1045–55.
[33] Lovibond O, et al. Numerical analysis of propellers for electric boats using computational fluid dynamics modelling. Energy Convers Manage: X 2023;17: 100349.
[34] Chen C, Delefortrie G, Lataire E. Effects of water depth and speed on ship motion control from medium deep to very shallow water. Ocean Eng 2021;231:109102.
[35] Lackenby H. The effect of shallow water on ship speed. Nav Eng J 1964;76(1): 21–6.
[36] Sharqawy M, Zubair S. Thermophysical properties of seawater: A review of existing correlations and data. Desalinat Water Treat 2010;16:354–80.
[37] Menter FR. Two-equation eddy-viscosity turbulence models for engineering applications. AIAA J 1994;32(8):1598–605.
[38] Koop A, Rossin B, Vaz G. Predicting wind loads on typical offshore vessels using CFD. ASME 2012 31st International Conference on Ocean, Offshore and Arctic Engineering. 2012.
[39] Larsen, S., The atmospheric Boundary Layer over land and sea: Focus on the offshore Southern Baltic and Southern North Sea region. 2013. 1-36.
[40] Yuck RH, Choi HS, Hong SY. Estimation of current loads on offshore vessels. The Fifteenth International Offshore and Polar Engineering Conference. 2005.
[41] Liu S, Papanikolaou A. On the prediction of the added resistance of large ships in representative seaways. Ships Offshore Struct 2017;12(5):690–6.
[42] Fang L, et al. Research on scale effect of ship appendage resistance based on CFD. The 29th International Ocean and Polar Engineering Conference. 2019. p. ISOPE-I-19-471.
[43] Zou Y, et al. Impacts of different characteristics of marine biofouling on ship resistance. Ocean Eng 2023;278:114415.
[44] Strasser G, et al. A verification of the ITTC/ISO speed/power trials analysis. J Mar Sci Technol 2015;20(1):2–13.
[45] Liu X, Zhao W, Wan D. Hull form optimization based on calm-water wave drag with or without generating bulbous bow. Appl Ocean Res 2021;116:102861.
[46] Díaz-Ojeda HR, Pérez-Arribas F, Turnock SR. The influence of dihedral bulbous bows on the resistance of small fishing vessels: A numerical study. Ocean Eng 2023; 281:114661.
[47] Tran TG, Van Huynh C, Kim HC. Optimal design method of bulbous bow for fishing vessels. Int J Nav Archit Ocean Eng 2021;13:858–76.
[48] Hakim ML, Suastika IK, Utama IKAP. A practical empirical formula for the calculation of ship added friction-resistance due to (bio)fouling. Ocean Eng 2023; 271:113744.
[49] García S, et al. Predicting ship frictional resistance due to biofouling using Reynolds-averaged Navier-Stokes simulations. Appl Ocean Res 2020;101:102203.
[50] Song S, et al. Investigating roughness effects on ship resistance in shallow waters. Ocean Eng 2023;270:113643.
[51] Piaggio B, et al. Z-Drive Escort Tug manoeuvrability model and simulation. Ocean Eng 2019;191:106461.